Supporting Information

Dynamic molecular tunnel junctions based on self-assembled monolayer for high tunneling current triboelectricity generation

Lu Zhang[1,2], Awad Shalabny[2], Chen Su[1], Xin Cui[3], Amro Sweendan[2], Kefan Zhang[2], Sherina Harilal[2], Sumesh Sadhujan[2], Muhammad Y. Bashouti [2,4]*

[1]*School of Advanced Materials and Nanotechnology, Xidian University, Shaanxi, 710126, P.R. China.*
[2]*Department of Solar Energy and Environmental Physics, Swiss Institute for Dryland Environmental and Energy Research, J. Blaustein Institutes for Desert Research, Ben-Gurion University of the Negev, Midreshset Ben-Gurion, Building 26, 8499000, Israel.*
[3]*School of Physics, University of Electronic Science and Technology of China, Chengdu 610054, P.R. China*
[4]*The IISe-Katz Institute for Nanoscale Science & Technology, Ben-Gurion University of the Negev, POB 653, Beer-Sheba Campus, Building 51, 8410501, Israel.*

Corresponding Author

Muhammad Y. Bashouti: *Bashouti@bgu.ac.il*

1. Pt-coated AFM tip work function calibration

The work function (WF) calibration of Pt-coated tip is a necessary process in HD-KPFM module, which has been conducted by using a standard highly oriented pyrolytic graphite (HOPG, defaulted WF = 4.6 ± 0.1 eV [1]). Fig. S1 shows the morphology of layer structure (Fig. S1a) and its corresponding surface potential mapping (Fig. S1b). According to the readout cross-section analysis line in Fig. S1c, the WF of Pt-coated tip can be up to 5.74 ± 0.01 eV, calculated by equation $CPD = SP_{tip} - SP_{sample}$.

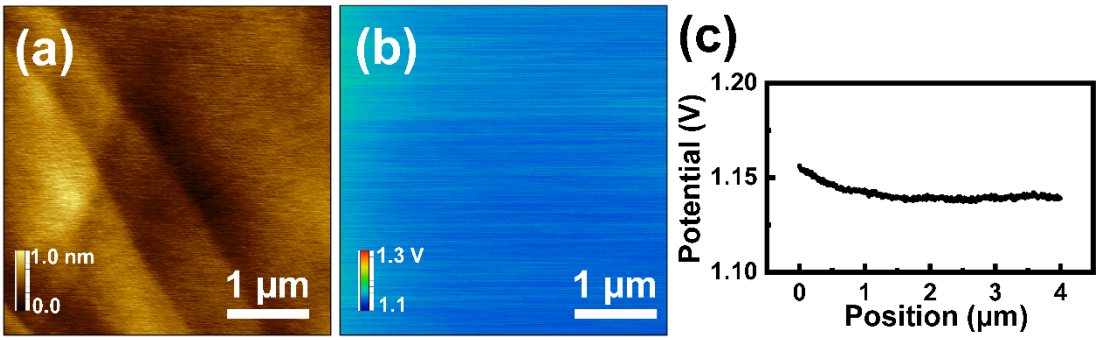

Fig. S1 Pt-coated AFM tip work function calibration. (a) Topographic image of HOPG and its corresponding surface potential (b), (c) readout cross-section analysis line from (b).

2. X-ray photoelectron spectroscopy (XPS) characterization

As shown in Fig. S2, the survey scan (Fig. S2a) shows signals from carbon, fluorine, gold, and sulfur, no other elements were detected. The high-resolution C 1s peak was fitted with 3 Gauss-Lorentz functions in Fig. S2b. The peak I located at 284.7 (marked as red) is characteristic of carbon atoms in the aromatic backbone, and the peak II located at about 285.2 eV (marked as yellow) is attributed to carbon bond to sulfur[2]. In addition, the peak III located at 286.2 eV (marked as green) is assigned to the shake-up process in the aromatic matrix[3]. Fig. S2c shows the F 1s peak located at 689.2 is assigned to the -CF_3 terminal group. The Au 4f patterns in Fig. S2d show that the intense doublet peak (marked as red) located at 84.7 eV and 88.4 eV are ascribed to the thiol SAM assembled on gold substrates and the weak doublet peak (marked as green) located at 85.2 eV and 89.1 eV might be assigned to atoms located at certain positions on the crystalline, faceted surfaces of nanoparticles[2]. The S 2p signal was fitted with two doublet peaks. The intense one located at 162.1 eV (marked as red) is attributed to sulfur bound to Au nanoparticles (Au-S) and the small one located at 163.5 eV (marked as green) is assigned to the sulfur of free thiol terminal (S-H)[4]. In general, the $PhSHCF_3$ monolayer was successfully assembled on the Au layer through Au-S covalent bond.

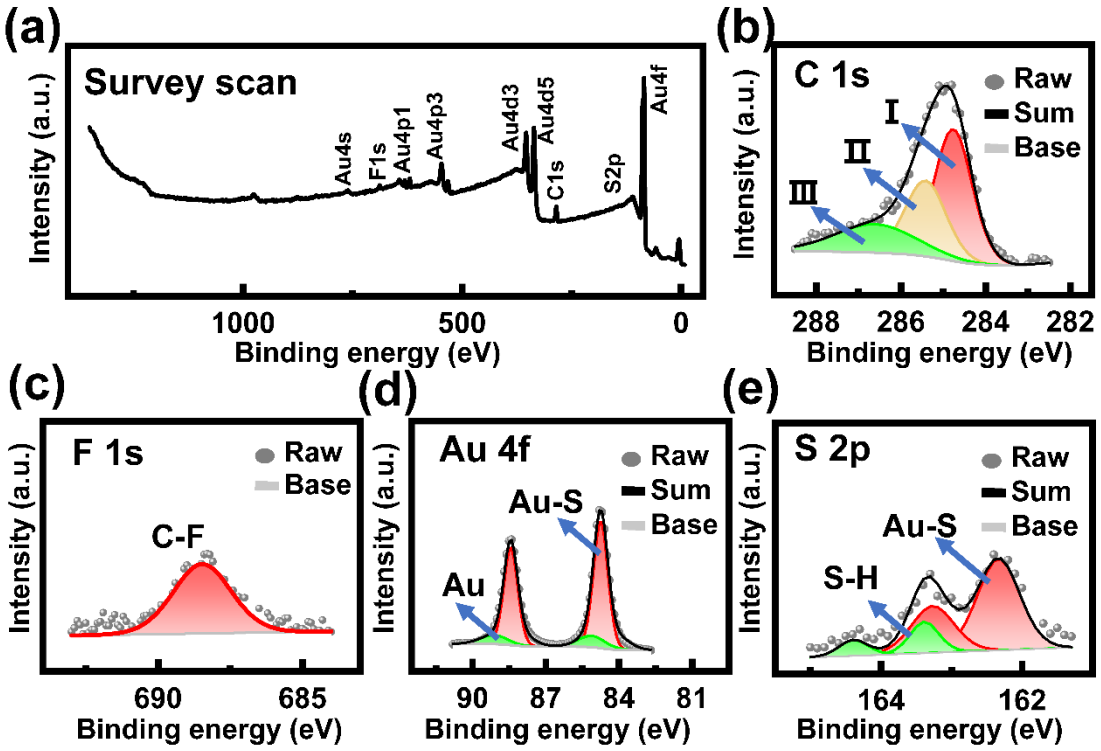

Fig. S2 XPS characterization of $PhSHCF_3$ chemically anchoring on Au film. (a) The survey scan, and its corresponding high resolutions C 1s (b), F 1s (d), Au 4f (e), and S 2p (f), are presented, respectively.

3. C-AFM calibration

The C-AFM module has been calibrated by verifying a series of standard resistors including 0.01, 1, and 100 MΩ provided by CSI AFM company. When the AFM probe was falsely engaged and contacted with resistors, a continuous bias ranging from -1.0 to 1.0 V was applied for the I-V test. As shown in Fig. S3, the slope of I-V curves agrees perfectly with the standard resistors' values, revealing no systematic error or artifact

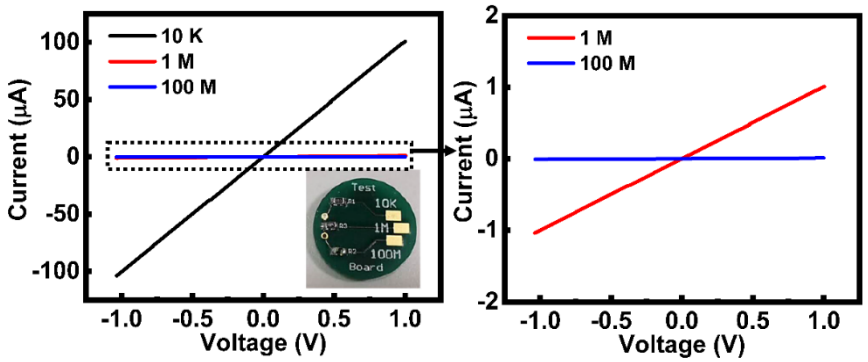

from the system.

Fig. S3 I-V characterization of standard resistors for C-AFM calibration.

4. C-AFM measurement on intrinsic Au layer

We have conducted C-AFM experiments on sputtering intrinsic Au film for comparison in this work. As shown in Fig. S4, evenly distributed sputtering Au film on a p^+-Si wafer (Fig. S4a), and the tunneling current signal (around tens of femtoamperes) can be ignored (Fig. S4b) under the driven velocity of 3.75 μm/s and the load pressure of 25 nN. Combining the experimental results in the text, it can convincedly prove that PhSHCF3 SAM plays an important role in the output tunneling current of DMIM structure.

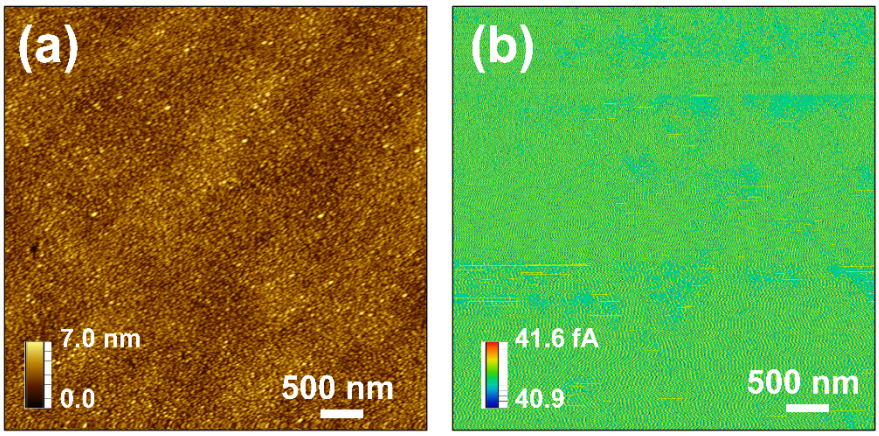

Fig. S4 Characterization of Pt-coated tip moving on intrinsic Au film for comparison.

5. FEM simulation

The FEM simulation of the electric field distribution at the tip-sample interface was

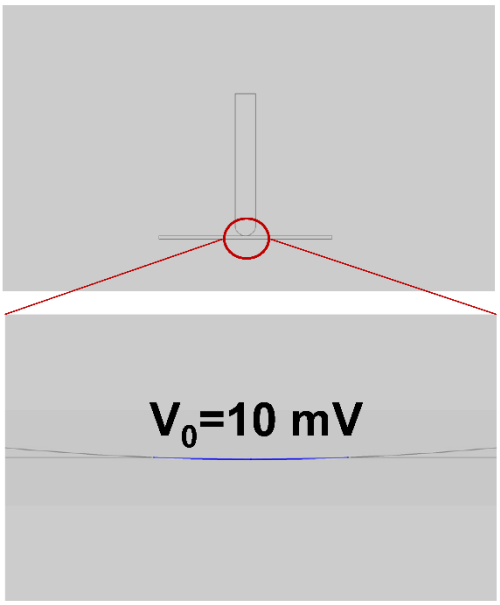

carried out using the 2D electrostatic module in the COMSOL Multiphysics software [5]. The $PhSHCF_3$ SAM was modelled by a 500 nm × 40 nm slab with a dielectric constant $\varepsilon = 2.94$ [6]. The tip has a conical shape with a spherical apex of 30 nm radius. A 1,500 nm × 1,500 nm slab was applied as an air atmosphere. The tip–sample contact was modelled by an indentation distance determined by the DMT model. While the initial electric potential $V_0 = 10$ mV was set at the tip–sample interface (Fig. S5), the rest of tip surface was assigned to be "zero charge" and the tip end was set to be the "ground" boundary condition.

Fig. S5 2D model for FEM simulation with an even distribution of 10 mV potential at the sample-tip interface.

6. Summarization of tutput performance of DC output generated based on various effects.

Table S1. Current density of DC output generated based on various effects

No.	Materials	Current ($A\ m^{-2}$)	Voltage (mV)	Impedance (MΩ)	Ref.
1	AFM Pt/Ir tip -MoS_2 nanosheets	10^6	7	10^3	[5]
2	AFM Pt/Ir tip -SiO_2 layer	10^4	---	10^5	[7]

3	Al film - n-type Si (Bulk)	40	600	10^{-3}	[8]
4	Gold-coated stick - SiO_2 layer on p-type Si	35	300	10^{3}	[9]
5	Stainless steel and n-type Si (Bulk)	10^{-1}~10^{-2}	10-20	10^{-3}	[10]
6	AFM Pt/Ir tip - graphite flake	10^{4}	135	10^{3}	[11]
7	AFM Pt/Ir tip - ZnO nanowires-packed film	10^{8}	5	10^{3}	[12]
8	AFM Pt/Ir tip-modified Si(211)	10^{9}	400	---	[13]
9	AFM Pt/Ir-SAM-Au	7.6◊10^{6}	10	10^{-2}	This work

7. C-AFM I-V spectras of different molecule thiols modified on Au films

For comparison, we have also conducted C-AFM measurements on other kinds of SAM on Au films including oligoacene thiols (thiophenol (PhSH), 4-tert-Butylbenzenethiol ($PhSHCH_3$), 4-(Dimerthylamino)benzenethiol ($PhSHNCH_3$) and $PhSHCF_3$) and alkane thiols (1-decanethiol ($C_{10}SH$) and 1-octadecanethiol ($C_{18}SH$)). As shown in Fig. S6, it shows different characteristics of I-V spectras caused by their nature attenuation factors and contact resistance.

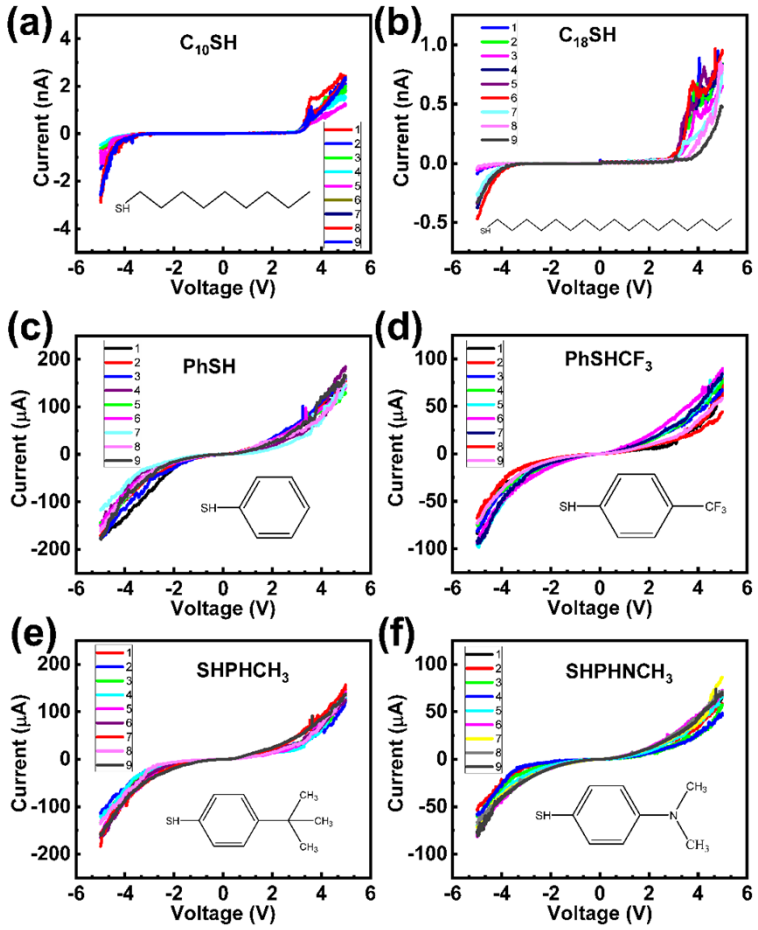

Fig. S6 C-AFM I-V spectras respecting to different molecule thiols modified on Au film. (a) $C_{10}SH$, (b) $C_{18}SH$, (c) PhSH, (d) $PhSHCF_3$, (e) $PhSHCH_3$, and (f) $PhSHNCH_3$. Here, nine different points are randomly collected from the surface (seen in legend for numbering). Insets of each graph show the corresponding chemical formula.

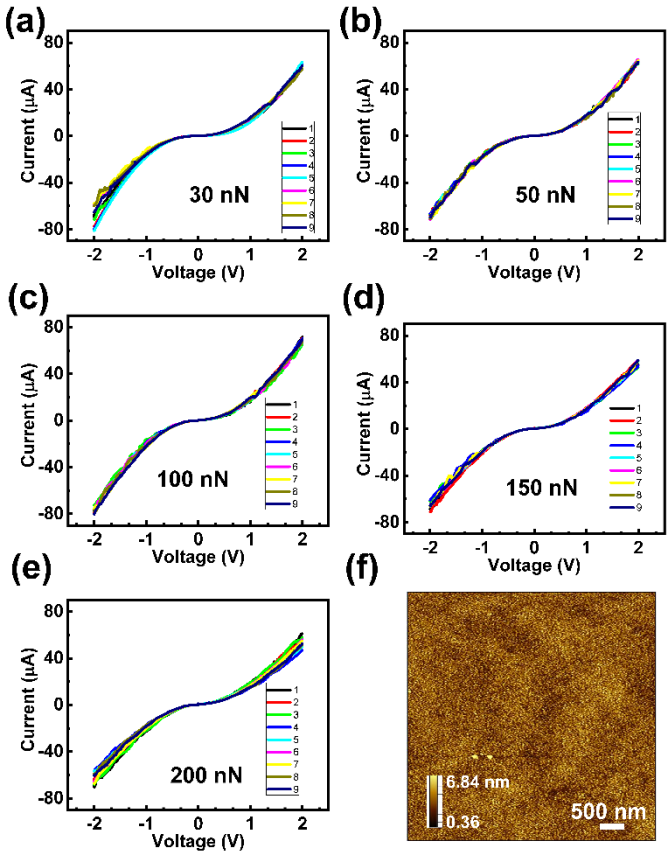

8. **Pressure resistance test on $PhSHCF_3$ modified Au layer**

Fig. S7 C-AFM I-V spectras respecting to different applied force on $PhSHNCH_3$ SAM. (a) 30 nN, (b) 50 nN, (c) 100 nN, (d) 150 nN, and (e) 200 nN. Here, nine different points are randomly collected from the surface (seen in legend for numbering). (f) the morphology of $PhSHNCH_3$ modified Au layer after 10 full-cycle scanning under 200 nN.

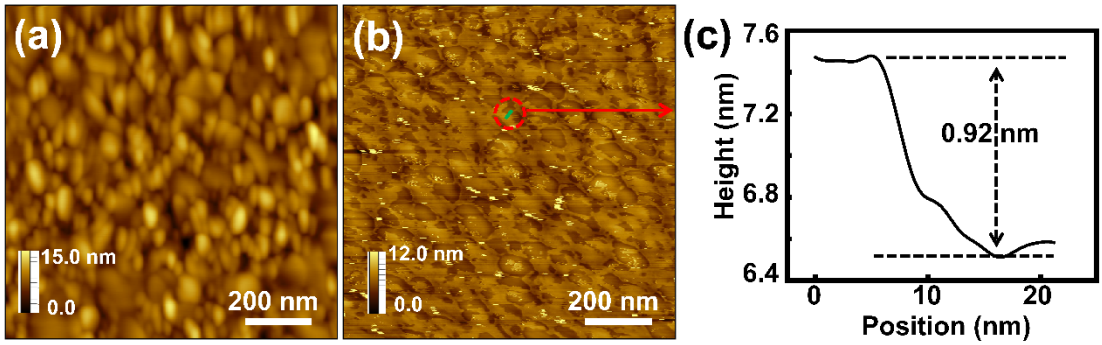

Fig. S8 Morphology characterization before (a) and after (b) intensive repetition scanning. (c) The thickness test of $PhSHCF_3$ SAM extracted from (b) is marked in a green line indicating the monolayer thickness of about 0.92 nm.

Regarding the thickness of $PhSHCF_3$ SAM, the monolayer thickness can be theoretically calculated at about 8.93 Å through molecular modeling within the Cambridge Scientific Chem3D software (MM2). Here, the molecular length is defined as the sum of the Au-S bond length (2.35 Å) and the distance between the terminal F atom on the $-CF_3$ to the S atom on the opposite end (6.58 Å)[3]. Furthermore, the thickness of $PhSHCF_3$ SAM also can be examined from Fig. S8b marked in the green line. The corresponding curve in Fig. S8c shows that the thickness of $PhSHCF_3$ SAM is about 0.92 nm, which is well agreed with the theoretical value.

9. Characterizations of Au nanoflakes

As is shown in Fig. S9a, the Au nanoflakes were synthesized through the hydrothermal approach depicted in the Methods section and stored in a 20 mL glass bottle until needed. The SEM image of a single triangle Au nanoflake (Fig. S9b) shows its side length is about 30 μm. To find a specific gold nanoplate before and after SAM modification quickly and accurately, we used a silicon substrate marked with a coordinate matrix in our experiment (Fig. S9c). After removing the native oxide in diluted HF buffer solution, the Au nanoflake solution was dropwise dropped on Si wafer and the Au nanoflake adhered to the substrate through van der Waals force. Fig. S9d demonstrates a typical Au nanoflake attached to the Si surface. In contrast, the I-V

curves were tested prior (Fig. S9e) and post (Fig. S9f) to the $PhSHCF_3$ SAM modification. Similar to the results from the sputtering Au film, the typical ohmic contact (before modification) can be completely changed into a symmetrical sigmoidal shape (post to modification) resulting from the nonresonant tunneling effect of $PhSHCF_3$ SAM.

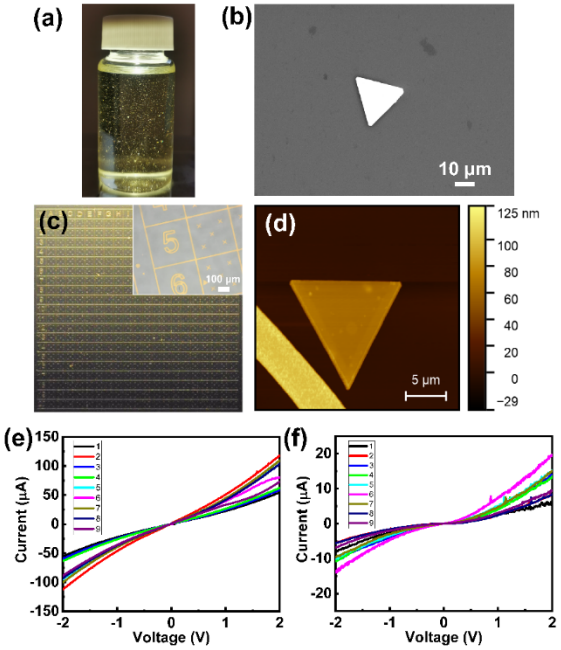

Fig. S9 Characterizations of Au nanoflakes and C-AFM I-V spectra. (a) Optical image of synthesized Au nanoflakes stored in a glass bottle. (b) SEM image of one Au nanoflake with triangle geometry. (c) Optical image of Au nanoflakes placed on one Si wafer with the coordinate matrix. Inset, partial enlargement of one coordinate. (d) Typical topographic image of one Au nanoflake. (e) and (f) C-AFM I-V spectras respecting prior and post to the $PhSHCF_3$ SAM modifications on Au nanoflake. Here, nine different points were collected from the surface (see legend for numbering).

10. Characterizations of flexible Au NW/PDMS electrode

According to the method introduced in the Methods section, we initially synthesized

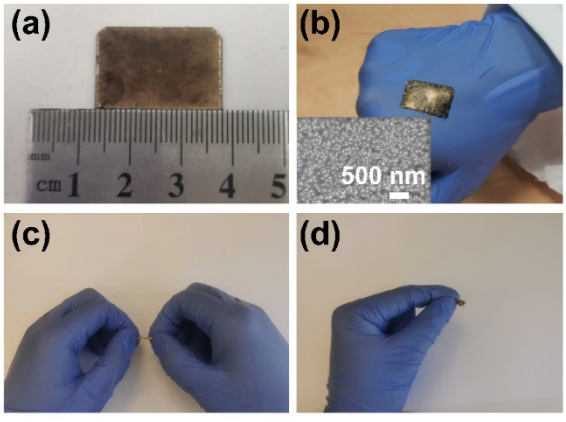

the Au seed-mediated nanowire array on the glass slide (Fig. S10a). After peeling off from the substrate, the Au NW/PDMS electrode can be conformally attached to the back of the hand, as shown in Fig. S10b. Furthermore, we also verify its mechanical performance such as the twist test (Fig. S10c) and foldable test (Fig. S10d). Finally, the flexible Au NW/PDMS electrode is suitable for macroscopic demonstration.

Fig. S10 Mechanical performance test of flexible Au NW/PDMS electrode. (a) Optical image of flexible Au NW/PDMS electrode fabricated on a glass slide. (b) Optical image of flexible Au NW/PDMS electrode attached on the back of the hand. Inset, SEM top-view image of the gold nanowire array. (c) Twist test and (d) foldable test of flexible Au NW/PDMS electrode.

Reference:

1. Melitz, W.; Shen, J.; Lee, S.; Lee, J. S.; Kummel, A. C.; Droopad, R.; Yu, E. T., Scanning tunneling spectroscopy and Kelvin probe force microscopy investigation of Fermi energy level pinning mechanism on InAs and InGaAs clean surfaces. *J. Appl. Phys.* **2010**, 108 (2), 023711.
2. Joseph, Y.; Besnard, I.; Rosenberger, M.; Guse, B.; Nothofer, H.-G.; Wessels, J. M.; Wild, U.; Knop-Gericke, A.; Su, D.; Schlögl, R.; Yasuda, A.; Vossmeyer, T., Self-assembled gold nanoparticle/alkanedithiol films: preparation, electron microscopy, XPS-analysis, charge transport, and vapor-sensing properties. *J. Phys. Chem. B* **2003,** *107* (30), 7406-7413.
3. Kim, B.; Choi, S. H.; Zhu, X. Y.; Frisbie, C. D., Molecular Tunnel Junctions Based on pi-Conjugated Oligoacene Thiols and Dithiols between Ag, Au, and Pt Contacts: Effect of Surface Linking Group and Metal Work Function. *J. Am. Chem. Soc.* **2011,** *133* (49), 19864-19877.
4. Mikhlin, Y.; Likhatski, M.; Tomashevich, Y.; Romanchenko, A.; Erenburg, S.; Trubina, S., Phenomena, R., XAS and XPS examination of the Au–S nanostructures produced via the reduction of aqueous gold (III) by sulfide ions. *J. Electron. Spectrosc. Relat. Phenom.* **2010,** *177* (1), 24-29.
5. Liu, J.; Goswami, A.; Jiang, K.; Khan, F.; Kim, S.; McGee, R.; Li, Z.; Hu, Z.; Lee, J.; Thundat, T., Direct-current triboelectricity generation by a sliding Schottky nanocontact on MoS_2 multilayers. *Nat. Nanotechnol.* **2018,** *13* (2), 112-116.
6. DelRio, F. W.; Steffens, K. L.; Jaye, C.; Fischer, D. A.; Cook, R. F., Elastic, adhesive, and charge transport properties of a metal-molecule-metal junction: the role of molecular orientation, order, and coverage. *Langmuir* **2010,** *26* (3), 1688-99.
7. Liu, J.; Miao, M.; Jiang, K.; Khan, F.; Goswami, A.; McGee, R.; Li, Z.; Lan, N.; Hu, Z.; Lee, J.; Cadien, K.; Thundat, T., Sustained electron tunneling at unbiased metal-insulator-semiconductor triboelectric contacts. *Nano Energy* **2018**, 48, 320-326.
8. Lin, S. S.; Lu, Y. H.; Feng, S. R.; Hao, Z. Z.; Yan, Y. F., A high current density direct-current generator based on a moving van der waals schottky diode. *Adv. Mater.* **2019**, 31 (7), 1804398.
9. Liu, J.; Jiang, K.; Lan, N.; Li, Z.; Thundat, T., Interfacial friction-induced electronic excitation mechanism for tribo-tunneling current generation. *Mater. Horiz.* **2019**, 6 (5), 1020-1026.
10. Zhang, Z.; Jiang, D. D.; Zhao, J. Q.; Liu, G. X.; Bu, T. Z.; Zhang, C.; Wang, Z. L.,

Tribovoltaic effect on metal-semiconductor interface for direct-current low-impedance triboelectric nanogenerators. *Adv. Energy Mater.* **2020**, 10(9), 1903713.
11. Huang, X.; Xiang, X.; Nie, J.; Peng, D.; Yang, F.; Wu, Z.; Jiang, H.; Xu, Z.; Zheng, Q., Microscale schottky superlubric generator with high direct-current density and ultralong life. *Nat. Commun.* **2021**, 12 (1), 1-10.
12. Song, Y.; Wang, N.; Fadlallah, M. M.; Tao, S.; Yang, Y.; Wang, Z. L., Defect states contributed nanoscale contact electrification at ZnO nanowires packed film surfaces. *Nano Energy* **2021**, 79, 105406.
13. Lyu, X.; Ferrie, S.; Pivrikas, A.; MacGregor, M.; Ciampi, S., Sliding Schottky diode triboelectric nanogenerators with current output of 10^9 A/m^2 by molecular engineering of Si(211) surfaces. *Nano Energy* **2022**, 102, 107658.